J Ther Eng, Vol. 10, No. 5, pp. 1253−1265, September, 2024

Journal of Thermal Engineering
Web page info: https://jten.yildiz.edu.tr
DOI: 10.14744/thermal.0000865

Research Article

Thermodynamic entropy of a magnetized nanofluid flow over an inclined stretching cylindrical surface

Mahesh GARVANDHA[1], Nagaraju GAJJELA[2,*], Vamsikrishna NARLA[3], Devendra KUMAR[4]

[1]*Mathematics and Computing Skills Curriculum and Assessment Unit, Preparatory Studies Center, University of Technology and Applied Sciences-Shinas, Muscat, 133, Sultanate of Oman*
[2]*Department of Mathematics, School of CSE (AIML), SR University, Hanamkonda District, Telangana, 506371, India*
[3]*GITAM School of Science, GITAM (Deemed to be University), Hyderabad, 502329, India*
[4]*Department of Information Technology, College of Computing and Information Sciences, University of Technology and Applied Sciences-Shinas, Muscat, 133, Sultanate of Oman*

ARTICLE INFO

Article history
Received: 30 September 2023
Revised: 03 December 2023
Accepted: 04 December 2023

Keywords:
Bejan Number, Entropy Generation, Inclined Stretching Cylinder, Nanofluid, Variable Thermal Conductivity

ABSTRACT

In the fluid transport processes extent of irreversibility causes entropy generation that leads to degrading the life span of any engineering system. The main objective of this investigation is to enhance the span of the system by analyzing the effects of various physical parameters. A nanofluid flow over an inclined stretching cylinder is studied to measure entropy generation due to thermal conductivity, Soret and Dufour effects along with viscous dissipation and internal heat source. Buongiorno model is considered as a base structure. The mathematical equations so formed are solved by shooting technique with Gill's fourth order method. Numerical results are validated with Homotopy analysis method through Bvph2.0. Effects of various parameters have been investigated on transport processes like axial velocity, temperature profile, and nanofluid concentration profiles. It seems that higher intensity of the applied magnetic field (M = 0, 1, 2), variable thermal conductivity (ε = 0.1, 0.3, 0.5), and Brinkman number (Br = 0.35) generates more entropy that degrades the system's life. Magnetic parameter and group parameter ($1 \leq Br/\Omega_1 \leq 3$), changing thermal conductivity all leads to a rise in entropy. In the study, group parameter reducing Bejan number that makes system more sustainable that full fills the aim of the study. Such physical situations generate more entropy must be reduced or avoided to make the system more efficient and long-lasting.

Cite this article as: Garvandha M, Gajjela N, Narla V, Kumar D. Thermodynamic entropy of a magnetized nanofluid flow over an inclined stretching cylindrical surface. J Ther Eng 2024;10(5):1253−1265.

***Corresponding author.**
*E-mail address: naganitw@gmail.com

This paper was recommended for publication in revised form by Editor-in-Chief Ahmet Selim Dalkılıç

INTRODUCTION

Nanofluid technology has emerged in recent years as a promising methodology to improve the thermal conductivity of the original fluid by mixing nanomaterials with the base fluid. Nanofluids have been implemented in electronics cooling, air conditioning, cancer therapy, and renewable energy systems. Many authors developed such innovative aspects and contributed massively to nanofluids. The term "nanofluid" was first proposed by Choi [1]. Buongiorno [2] contributed conservation equations in nanofluid that are based on these two mechanisms of random motion of air bubbles in still air and a kind of force generated by heat air and cool wall of particles. Nield and Kuznetsov [3] applied the Buongiorno model to investigate the patterns of nanofluid flow that is porous in nature and the flow is passing through a vertical plate. The used nanofluid contains sub-microsonic solid particles that create porosity in the medium. Meantime, distinct boundary layer conditions were incorporated in the studies done by Mansur and Ishak [4], Kuznetsov and Nield [5]. Rana and Thakur [6] used the Buongiorno model and noticed critical values for the existence of the dual solution along an inclined stretching cylinder. Recently, V.K. Narla et al. [7] investigated the transport of nanofluid flow using electroosmosis in a curved channel. Magnetohydrodynamic (MHD) nanofluid flow has numerous applications like those of the earth generated heat energy eradication, nuclear reactors, and the petroleum industry. The MHD nanofluid flow with different geometries has been focused on by several authors (Mahatha et al. [8], Nagaraju et al. [9], Mondal et al. [10] and Kandwal et al. [11]).

The transport of heat from one solid medium or place to another is studied as thermal conductivity. The phenomenon of thermal transport is very common in every fluid transfer process. Elbashbeshy et al. [12] studied the impact of heat treatment of materials with time-dependent nanofluid flows in moving cylinders. Bisht et al. [13] studied mixed convection to investigate the effects of chemical reactions and heat transport of variable nature on fluid flows through long cones of circular geometry. Some theoretical and experimental studies by Ravi Kanth and Kumar [14] have provided close correction with variation in temperature with thermal conductivity. The most significant properties of variable thermal conductivity for stretching cylinder is working with different nanofluids are reported in (Salahuddin et al. [15], Ramzan et al. [16], and Gajjela and Garvandha [17]).

Boundary layer theory plays a significant role in fluid flow systems. Sakiadis [18] initiated to examine the behavior of boundary layer flow along rigid surfaces. The author suggested this boundary layer flow for both laminar and turbulent flow. Crane [19] developed a model for steady, quiescent, two-dimensional flow along a stretching sheet moving with linearly varying speed followed by Sakiadis [18]. After that many researchers examined various aspects of the boundary layer flow along continuous and finite rigid surfaces and came up with some interesting results. Wang [20] explored the steady, continuous 2-dimensional fluid flow in stretching cylinder in outer stretched surfaces. Gorla et al. [21] studied phase change(melting) condition at cylindrical wall for nanoparticle heat transfer flow. Dhanai et al. [22] used the Buongiorno model to analyze the slip effects over an inclined stretching cylinder. The impacts of Thermo-diffusion and Diffuso-thermal in mixed systems, which are frequently encountered in chemical engineering applications, are noteworthy for coupled heat, and mass transport would be much more substantial if the fluid medium is kept at lower density compared to the surrounding medium by suspending chemical species. In numerous chemical processes, there is indeed a chemical species that involves latent mass transport. These processes can be found in a variety of industrial challenges, such as ceramics production, glassware industry, food processing, polymer production, and many more. EL-Kabeir [23] examined the effects of Cross-diffusions within existence of a chemical reaction over a stretching cylinder which is embedded in the porous medium. Dzulkifli et al. [24] studied nanofluid transport to identify Soret and Dufour effect over stretching/shrinking sheet. Some of the interesting results on Cross-diffusions with different flow geometry have been reported in previous studies (Gajjela et al. [25], Jain and Bohra [26], Gajjela and Garvandha [27], Idowu and Falodun [28]).

Entropy-generation minimization is required from the engineering point of view and sustains the long life of the system. Bejan and Kestin [29] invented the entropy generation minimization approach and suggested its wide use in research, engineering, and industrial applications. Butt et al. [30] developed a theoretical model for entropy in the transport of Newtonian fluid over a stretching cylinder. Srinivasacharya and Shafeeurrahman [31] investigated the entropy generation in a nanofluid flow in concentric cylinders. Some of the impressive papers in entropy generation analysis for various fluids with diverse geometries can even be found in previous studies (Taghizadeh and Asaditaheri [32], Tufail et al. [33], Zheng et al. [34], Jha and Yusuf [35]). Recently Sahoo and Nandkeolyar [36] investigated the mixed convective flow of Casson nanofluid. The authors studied entropy generation and loss of heat energy. Thermal radiations and hall current effects are seen in entropy generation. Specific quasi-linearization and chebyshev collocation method is used to observe the effects of various parameters. Zahor et al. [37] suggested a review of the previously established models for irreversibility in magnetohydrodynamics (MHD) nanofluid transport systems. The authors used numerical methods to solve the equations in their modeling. Ankush Raje et al. [38] analyzed the entropy generation for viscoelastic Jeffery fluid transport through an inclined circular pipe. They considered the porous fluid medium

under constant pressure and applied a uniform magnetic field to the system. The finite difference approach is used in the mathematical solution. Copper nanoparticles are studied with blood due to low cost and other factors. Teh and Asghar [39] carried out investigations on MHD hybrid nanofluid transport in three dimensions through a shrinking/rotating sheet that is rotating. In the application of Joule heating effects authors reported that there is a significant proportion with the transport profiles, hybrid nanofluid, heat, and rotating parameters. Ferroudj et al. [40] examined the square cavity filled with fluid for mixed convection for finding facts for entropy generation due to irreversibility distribution ratio with Prandtl numbers. The authors have significantly quoted the irreversibility distribution ratio increases the entropy generation for all Prandtl numbers like the fluids under certain thermal conditions, air (mixture of gases), and water.

Most recently, Sharma et al. [41] investigated entropy optimization for micropolar ternary hybrid nanofluid flow of blood. The authors have studied Bayesian regularization networks with homogeneous as well as heterogeneous chemical reactions. Mishra et al. [42] investigated the nanofluid flow behaviour in arteries having stenosis. The flow patterns and their impacts are seen with MHD applications. Paul et al. [43] investigated the flow rates for hybrid nano fluids over the nanofluids. The hybrid nanofluid is flowing through a vertically stretching cylinder. The authors found that thermal behaviors of hybrid nanofluid is significantly better over nanofluids as the thermal transport enhances up to 7.5% more under the impact of thermal stratification.

The previously reported literature encourages validating the existing entropy optimization and understanding the variations in transport phenomenon due to various parameters reported. The findings listed above reveal that not much more has been reported on the second law analysis over a stretching cylinder with heat and mass transfer. Such attempts at varying a fluid's thermal conductivity have not been demonstrated. Motivated by this fact, we seek to quantitatively investigate the impacts of entropy, Soret, and Dufour across an inclined stretching cylinder in nanofluid flow with chemical reaction, heat generation.The non-dimensional equations are solved by an efficient algorithm NDSolve in MATHEMATICA and validated the solutions with Bvph2.0 which is based on Homotopy analysis method developed by Zhao and Liao [44].

MATHEMATICAL FORMULATION

Let us consider a 2-dimensional, time independent, boundary layer flow of incompressible nanofluid due to an inclined stretching cylinder of radius a. A magnetic field B_0 normally gets applied to the stretching surface. The physical model and coordinates system are depicted in Figure 1. The cylindrical coordinates are employed, with the z -axis aligned with the axial direction and the r -axis aligned with the cylinder's normal. Furthermore, the energy equation is taken into account with the combined effects of heat source and viscous dissipation. The thermal conductivity varies with temperature.

The Cross-diffusions (Thermo-diffusion and Diffusothermal) effects are put into consideration, and the flow region is governing with a homogeneous chemical reaction of first-order. The continuity, momentum, energy, and concentration equations of nanofluid flow after using boundary layer approximation with the stated assumptions are written as [27, 30, 33]:

$$\text{Continuity Equation:}\frac{\partial u}{\partial r}+\frac{u}{r}+\frac{\partial w}{\partial z}=0 \tag{1}$$

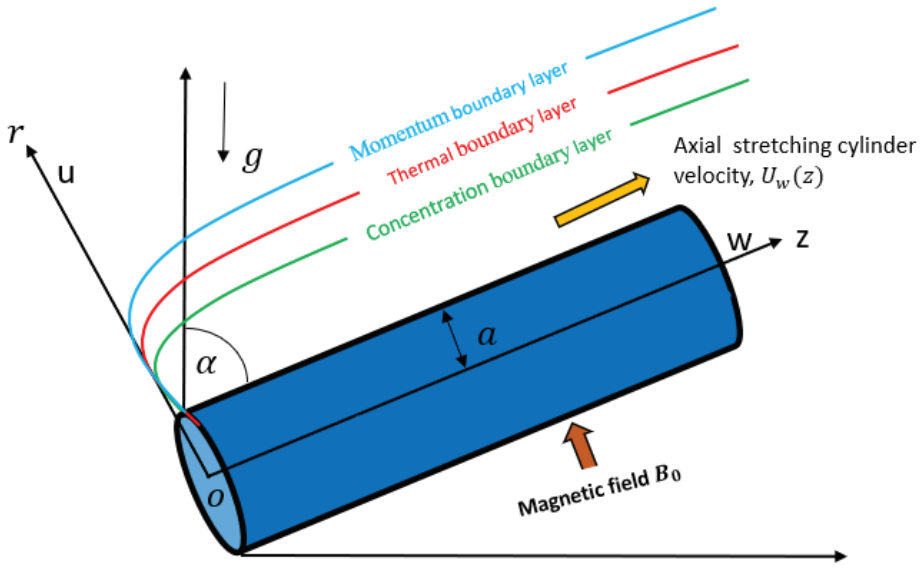

Figure 1. Schematic diagram.

Momentum equation:

$$u\frac{\partial w}{\partial r}+w\frac{\partial w}{\partial z}=\frac{\mu}{\rho}\frac{1}{r}\frac{\partial}{\partial r}\left(r\frac{\partial w}{\partial r}\right)-\frac{\sigma {B_0}^2 w}{\rho}+g\left(\beta_T(T-T_\infty)+\beta_c(C-C_\infty)\right)cos\alpha \quad (2)$$

Thermal energy Equation:

$$\rho C_p\left(u\frac{\partial T}{\partial r}+w\frac{\partial T}{\partial z}\right)=\frac{1}{r}\frac{\partial}{\partial r}\left(k(T)r\frac{\partial T}{\partial r}\right)+\rho^* C_p^*\left(D_B\frac{\partial T}{\partial r}\frac{\partial C}{\partial r}+\frac{D_T}{T_\infty}\left(\frac{\partial T}{\partial r}\right)^2\right)+\mu\left(\frac{\partial w}{\partial r}\right)^2+Q_0(T-T_\infty)+\frac{\rho D K_T}{C_s C_p}\left(\frac{\partial^2 C}{\partial r^2}+\frac{1}{r}\frac{\partial C}{\partial r}\right) \quad (3)$$

Concentration Equation:

$$u\frac{\partial C}{\partial r}+w\frac{\partial C}{\partial z}=\frac{D_B}{r}\frac{\partial}{\partial r}\left(r\frac{\partial C}{\partial r}\right)+\frac{D_T}{T_\infty}\frac{1}{r}\frac{\partial}{\partial r}\left(r\frac{\partial T}{\partial r}\right)+\frac{DK_T}{T_m}\left(\frac{\partial^2 T}{\partial r^2}+\frac{1}{r}\frac{\partial T}{\partial r}\right)-K_1(C-C_\infty) \quad (4)$$

Below are the boundary conditions defined for the above model:

$$w=U_w(z),\quad u=0,\quad T=T_w,\quad D_B\frac{\partial C}{\partial r}+\frac{D_T}{T_\infty}\frac{\partial T}{\partial r}=0\ at\ r=a, \quad (5)$$

$$w\to 0,\ T\to T_\infty,\ C\to C_\infty\ as\ r\to\infty, \quad (6)$$

where $U_w(z)=\frac{U_0 z}{l}=$ stretching cylinder velocity, $T=T_w=T_\infty+T_0\frac{z}{l}$ prescribed surface temperature, $C=C_w=C_\infty+C_0\frac{z}{l}$. U_0, T_0, C_0 are the reference velocity, temperature, and concentrations respectively, T_∞, C_∞ is the ambient temperature and concentrations respectively.

Let us consider the set of similarity transformation and non-dimensional variables [27, 30, 33] as

$$w=\frac{U_0 z}{l}f',u=\frac{-a}{r}\left(\frac{U_0\nu}{l}\right)^{\frac{1}{2}}f(\eta),\eta=\frac{r^2-a^2}{2a}\left(\frac{U_0}{\nu l}\right)^{\frac{1}{2}},$$
$$\theta(\eta)=\frac{T-T_\infty}{T_w-T_\infty},\ \phi(\eta)=\frac{C-C_\infty}{C_w-C_\infty},\ M^2=\frac{\sigma {B_0}^2 l}{\rho U_0},$$
$$\gamma=\left(\frac{\nu l}{a^2 U_0}\right)^{\frac{1}{2}},Gr_t=\frac{g\beta_T(T_w-T_\infty)l^2}{{U_0}^2 z},\ Gr_c=\frac{g\beta_C(C_w-C_\infty)}{{U_0}^2 z},$$
$$Pr=\frac{\mu c_p}{k_\infty},Nb=\frac{\rho^* C_p^* D_B(C_w-C_\infty)}{\rho C_p\nu},\ Nt=\frac{\rho^* C_p^* D_T(T_w-T_\infty)}{T_\infty\rho C_p\nu},$$
$$Ec=\frac{U_w^2}{c_p(T_w-T_\infty)},Br=Pr*Ec,\ Q=\frac{Q_0 l}{\rho C_p U_0},\ Sr=\frac{DK_T T_0}{\nu T_m C_0},$$
$$Df=\frac{DK_T C_0}{\nu C_s C_p T_0},\ Sc=\frac{\nu}{D_B},\ C_r=\frac{Kl}{U_0}. \quad (7)$$

The Equation (1) is verified by the aforementioned similarity transformations, and the corresponding governing equations of (2)-(6) are transformed by using the similarity variables in Equation (7). The obtained equations with boundary conditions are as follows:

$$(1+2\eta\gamma)f'''+2\gamma f''+ff''-(f')^2-M^2f'+(Gr_t\theta+Gr_c\phi)cos\alpha=0, \quad (8)$$

$$(1+2\eta\gamma)\theta''+2\gamma\theta'+\varepsilon\{(1+2\eta\gamma)(\theta'^2+\theta\theta'')+2\gamma\theta\theta'\}+Pr(f\theta'-f'\theta+Q\theta)+Pr(1+2\eta\gamma)\{Nb\theta'\phi'+Nt\theta'^2\}+Br(1+2\eta\gamma)(f'')^2+Df\ Pr\ ((1+2\eta\gamma)\phi''+2\gamma\phi')=0, \quad (9)$$

$$(1+2\eta\gamma)\phi''+2\gamma\phi'+Sc(f\phi'-f'\phi)+\frac{Nt}{Nb}\left((1+2\eta\gamma)\theta''+2\gamma\theta'\right)-C_r Sc\phi+Sc\ Sr\ ((1+2\eta\gamma)\theta''+2\gamma\theta')=0, \quad (10)$$

$$f(\eta)=0,\ f'(\eta)=1,\ \theta(\eta)=1,\ Nb\phi'(\eta)+Nt\theta'(\eta)=0\ \ at\ \eta=0, \quad (11)$$

$$f'(\eta)=0,\theta(\eta)=0,\phi(\eta)=0\ \ as\ \eta\to\infty. \quad (12)$$

The physical quantity of interests C_f (Skin-friction coefficient), *Nu* (Nusselt number), and *Sh*(Sherwood number) are, in terms of similarity variables, given by:

$$\frac{1}{2}C_f\sqrt{Re_z}=-f''(0),\frac{Nu_z}{\sqrt{Re_z}}=-\theta'(0),\frac{Sh_z}{\sqrt{Re_z}}=-\phi'(0), \quad (13)$$

where $Re_z=\frac{U_w z}{\nu}$

The entropy generation [29] is derived as follows:

$$S_G=\frac{k(T)}{T_\infty^2}\left(\frac{\partial T}{\partial r}\right)^2+\frac{\mu}{T_\infty}\left(\frac{\partial w}{\partial r}\right)^2+\frac{R_U D}{C_\infty}\left(\frac{\partial C}{\partial r}\right)^2+\frac{R_U D}{T_\infty}\frac{\partial T}{\partial r}\frac{\partial C}{\partial r}+\frac{\sigma B_0^2}{T_\infty}w^2. \quad (14)$$

Equation (14) clearly depicts the entropy effects generated by heat transfer (*HT*), fluid friction (*FF*), diffusion (*DF*), and magnetic field (*MF*). In dimension-less form, the entropy generation number is

$$Ns=\frac{S_G}{S_C}=\frac{Re}{Z}(1+\varepsilon\theta)(1+2\eta\gamma)(\theta')^2+\frac{Re}{Z}(1+2\eta\gamma)\frac{Br}{\Omega_1}(f'')^2+\frac{Re}{Z}(1+2\eta\gamma)\phi_1(\phi')^2+\frac{Re}{Z}(1+2\eta\gamma)\phi_2\theta'\phi'+\frac{Re}{Z}\frac{Br}{\Omega_1}M^2(f')^2, \quad (15)$$

$$Ns=Ns_{HT}+Ns_{FF}+Ns_{DF}+Ns_{MF},$$

where $S_C=\frac{k_\infty(T_w-T_\infty)^2}{T_\infty^2 l^2},\ Re=\frac{Ul}{\nu},\quad \Omega_1=\frac{T_w-T_\infty}{T_\infty},$
$Br=Pr\,Ec,\ \phi_1=\frac{R_U D\,T_\infty}{k_\infty(T_w-T_\infty)}\frac{\Omega_2}{\Omega_1}\Delta c,\phi_2=\frac{R_U D}{k_\infty\Omega_1}\Delta C,$
$\Delta C=C_w-C_\infty,\ \Omega_2=\frac{C_w-C_\infty}{C_\infty},\ Z=\frac{z}{l}.$

The Bejan number (*Be*) [29] is expressed as

$$Be=\frac{Ns_{HT}}{Ns_{HT}+Ns_{FF}+Ns_{DF}+Ns_{MF}} \quad (16)$$

RESULTS AND DISCUSSION

The numerical solutions of highly nonlinear, coupled, boundary value problems (8)-(12) are attained by Shooting technique with fourth order Runge-Kutta-Gill method. Further the obtained numerical results are validated by Liao's Homotopy Analysis method using Bvph2.0

in MATHEMATICA. The asymptotic boundary conditions in Equation (12) as $\eta \to \infty$ are substituted for those at such a large but finite value of $\eta = 6$.

Figures 2 to 4 show the axial velocity variation for variant values of γ, M, and α. It is clear that the axial velocity rises with an increase of γ. Away from the axis of the cylinder, the rate of transfer declines until it eventually disappears. In Figure 3(a), as M increases, the axial velocity decreases. This is due to Lorentz force which causes the reduction in the fluid velocity, and it increases the temperature. Figure 4(a) illustrates the axial velocity declining as α changes from $\pi/6$ to $\pi/3$. This is due to the maximum gravitational force

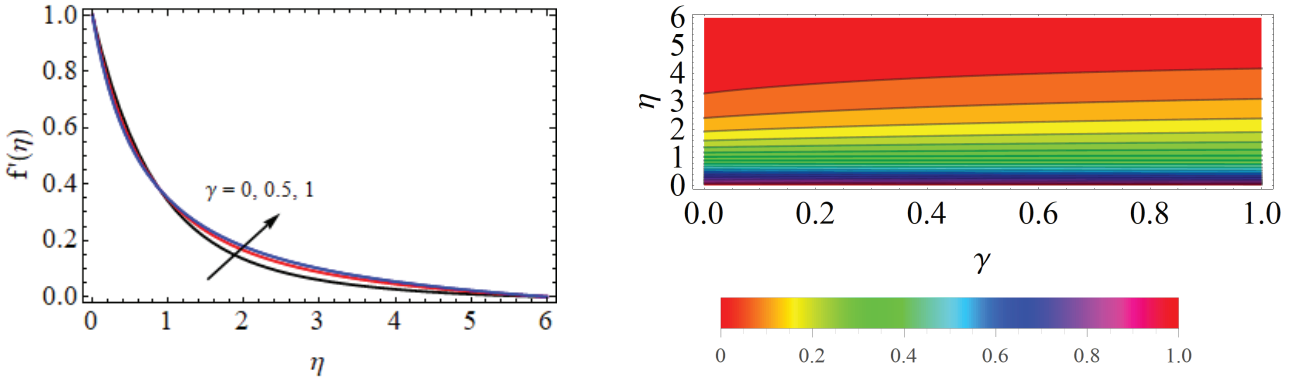

(a) (b)

Figure 2. Axial velocity variation with (a) distinct γ values (b) contour plot, when $Pr = 0.7$; $M = 1$; $Gr_t = 0.3$; $Gr_c = 0.3$; $\alpha = \pi/4$; $Q = 0.3$; $\varepsilon = 0.1$; $Nb = 0.1$; $Nt = 0.1$; $Br = 0.35$; $Df = 0.5$; $Sc = 0.5$; $Sr = 0.5$; $C_r = 0.3$.

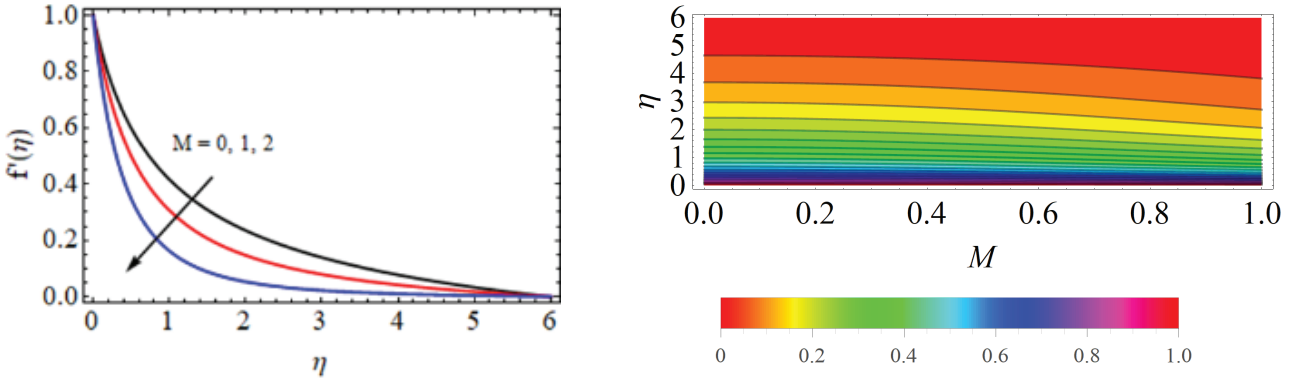

(a) (b)

Figure 3. Axial velocity variation with (a) distinct M values (b) contour plot.

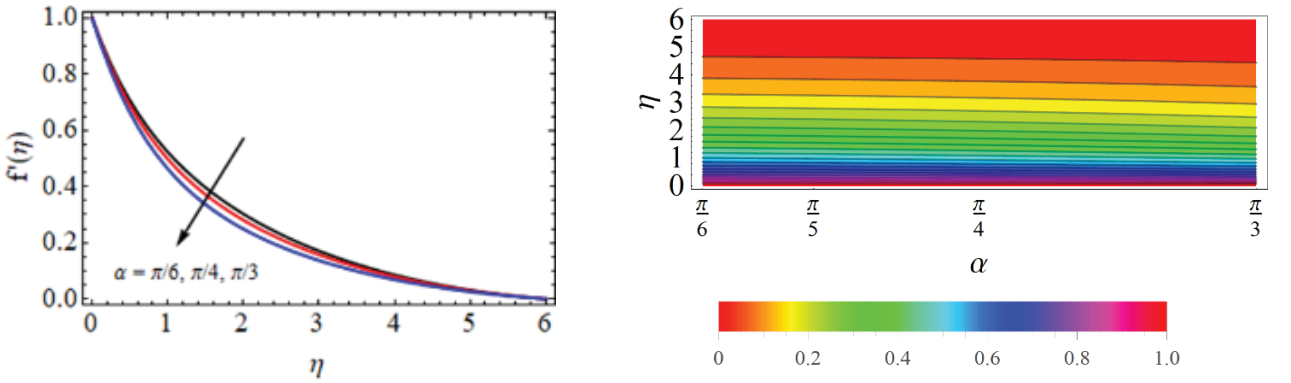

(a) (b)

Figure 4. Axial velocity variation with (a) distinct α values (b) contour plot.

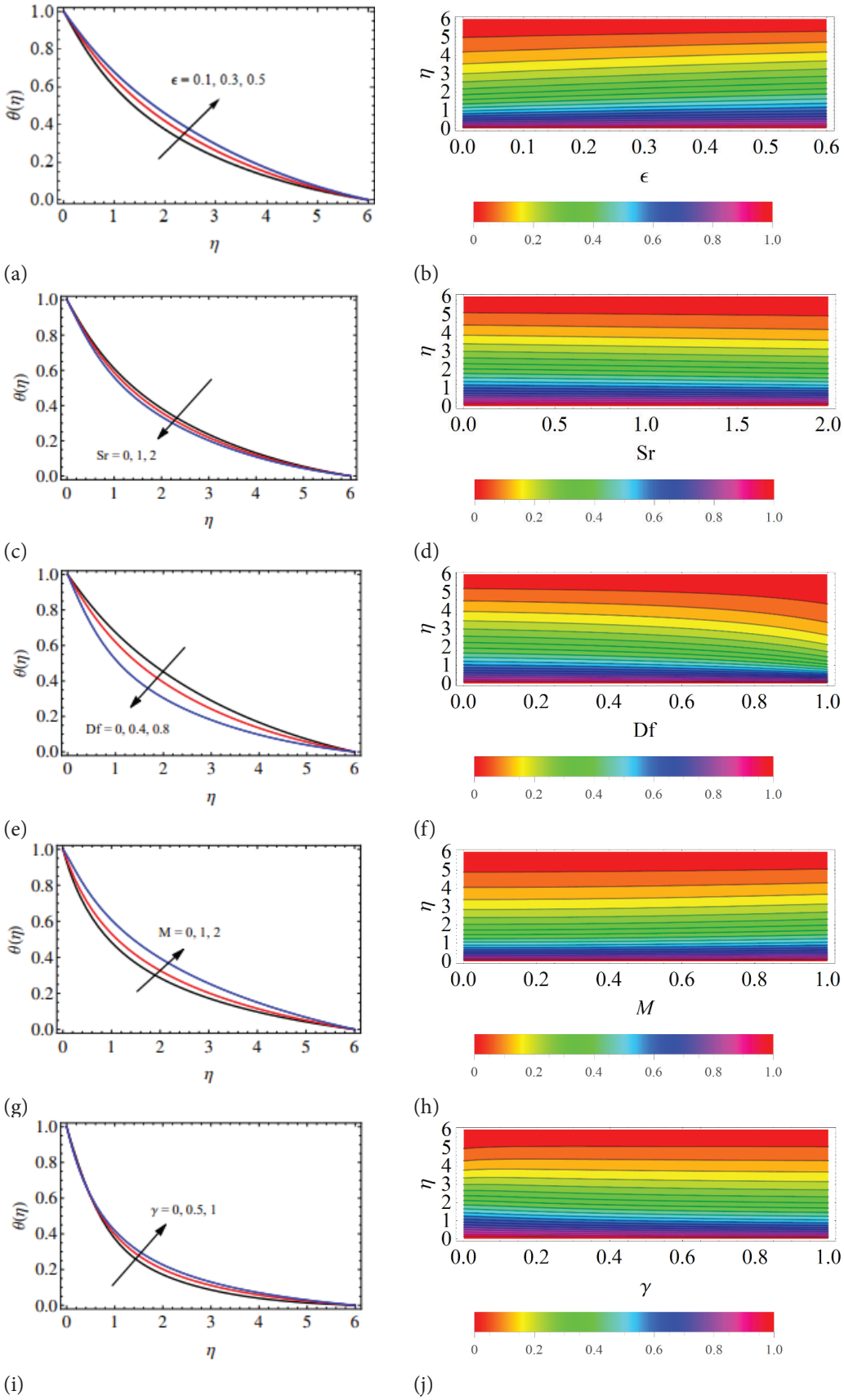

Figure 5. Temperature profile for (a) distinct ε values (b) contour plot (c) distinct *Sr* values (d) contour plot (e) distinct *Df* values (f) contour plot (g) distinct *M* values (h) contour plot (i) distinct γ values (j) contour plot , when $\gamma = 0.2$; $Pr = 0.7$; $M = 1$; $Gr_t = 0.3$; $Gr_c = 0.3$; $\alpha = \pi/4$; $Q = 0.3$; $\varepsilon = 0.1$; $Nb = 0.1$; $Nt = 0.1$; $Br = 0.35$; $Df = 0.5$; $Sc = 0.5$; $Sr = 0.5$; $C_r = 0.3$

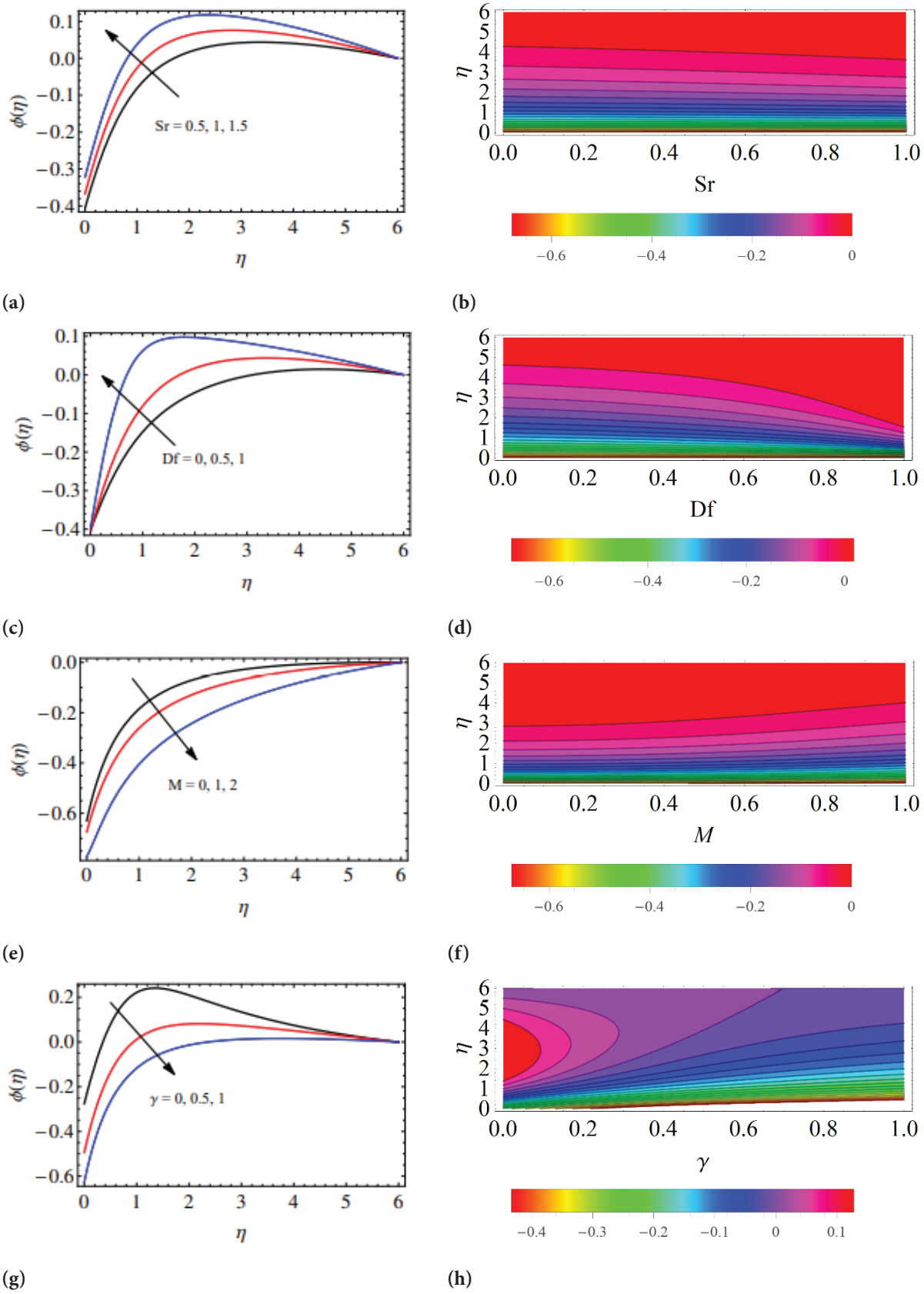

Figure 6. Concentration profile for (a) distinct *Sr* values (b) contour plot (c) distinct *Df* values (d) contour plot (e) distinct *M* values (f) contour plot (g) distinct γ values (h) contour plot , when $\gamma = 0.2$; $Pr = 0.7$; $M = 1$; $Gr_t = 0.3$; $Gr_c = 0.3$; $\alpha = \pi/4$; $Q = 0.3$; $\varepsilon = 0.1$; $Nb = 0.1$; $Nt = 0.1$; $Br = 0.35$; $Df = 0.5$; $Sc = 0.5$; $Sr = 0.5$; $Cr = 0.3$.

experienced by the fluid and consequently, the velocity and the thickness of the boundary layer dropped significantly.

Figure 5 depicts the temperature profile variation for different values of ε, *Sr, Df, M*, *γ*. From Figures 5(a) and 5(b), we can see that temperature increases with variable thermal conductivity (ε). This is due to our assumption that the thermal conductivity varies linearly with temperature. The transverse velocity is reduced, and the temperature profile rises as the variable thermal conductivity parameter increases. The temperature decelerates with increasing values of Soret (*Sr*) and Dufour number (*Df*) is shown in Figures 5(c)-5(f). Physically, *Sr* and *Df* provide a thermal and concentration gradient, respectively, which results in a decreased convective flow and a corresponding drop in temperature. In Figure 5(g), as M increases, the temperature increases. This is due to Lorentz force which causes the reduction in the fluid velocity and it increases the temperature. Temperature shows the rising trends with higher values of *γ* in Figure 5(i). As there will be an inverse proposition between curvature and radius, higher curvature leads to a reduction of the cylinder surface area.

Figure 6 illustrates the concentration profile variation for different *Sr, Df, M*, and *γ*. We can see that from Figures 6(a)-6(d) concentration field enhances when Soret number (*Sr*), and Dufour number (*Df*) increases. The considered higher numerical values of *Sr* and *Df*, results in a stronger convective flow that increases in concentration profile but in case of magnetic parameter and curvature parameter, the concentration profile decelerates as shown in Figures 6(e)-6(h). The reduced surface area enhances fluid flow over the surface, temperature, and decelerating concentration.

To analyze the thermodynamic second law for this problem, the graphs (contour plots) are portrayed for entropy generation number (*Ns*) and Bejan number (*Be*) in Figures 7, 8. Figure 7(a) exhibits that the group parameter (Br/Ω_1) increases, the *Ns* increases. If the value of the group parameter rises, fluid friction, and magnetic field influence the entropy effects of heat transfer on the stretching pipe. Yet, in the case of expanding pipe, such results are not in absolute control. It is evident from Figures 7(b)-7(d) that entropy generation number increases for ε, *M* and *γ*. Due to the magnetic force's resistive nature, *Ns* increases as *M* increases. We can minimize entropy generation by weakening the magnetic field.

The impacts of entropy begin to depreciate as one moves away from the surface, as shown in Figure 7(c). Figure 8 reveals that the maximum value of Bejan number is 1. Bejan number decreases with group parameter (Br/Ω_1) and increases for ε, *M* and *γ*. The graph (8(c)-8(d)) shows that as *M* increases, heat transfer irreversibility at the surface of

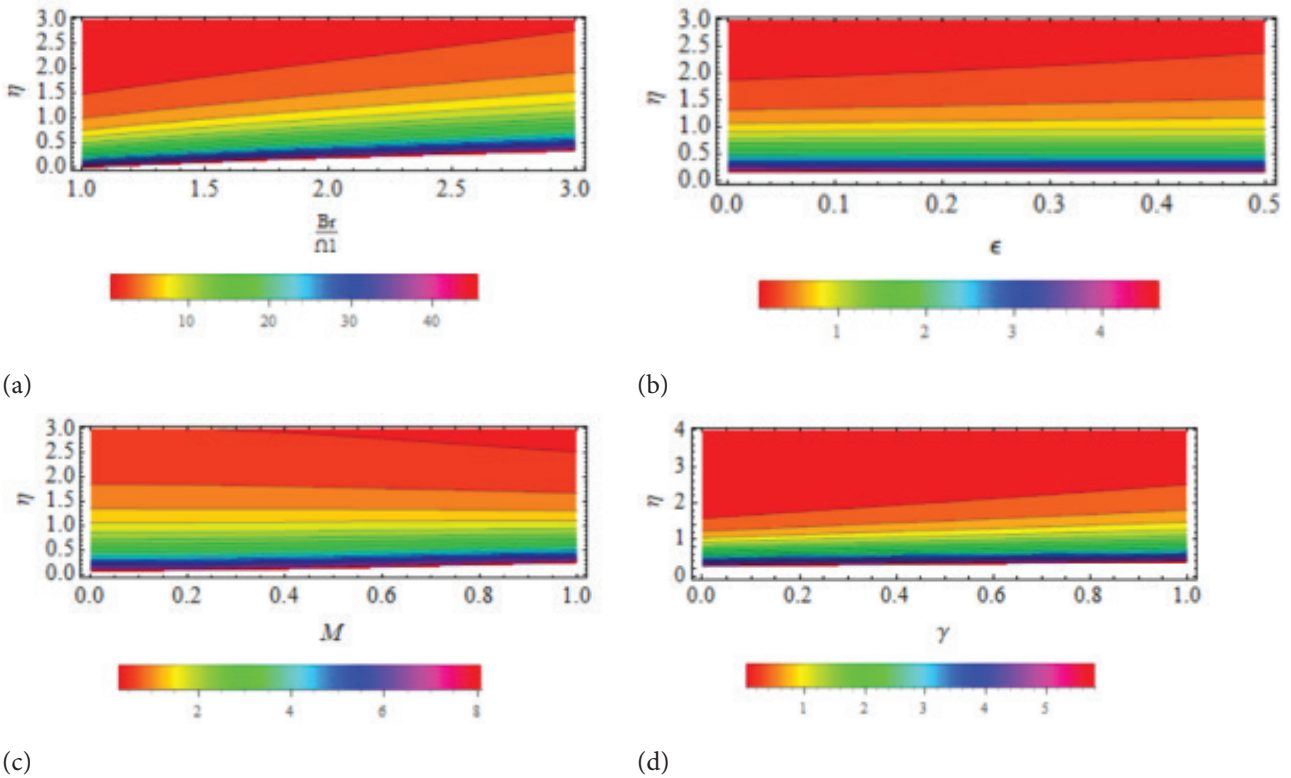

Figure 7. Contour plot for Average entropy generation rate for (a) distinct modified Brinkman number (b) distinct ε (c) distinct *M* (d) distinct *γ*, when $Gr_t = 0.3$; $Gr_c = 0.3$; $\alpha = \pi/4$; $Q = 0.3$; $\varepsilon = 0.1$; $Nb = 0.1$; $Nt = 0.1$; $Br = 0.35$; $Df = 0.5$; $Sc = 0.5$; $Sr = 0.5$; $C_r = 0.3$; $\gamma = 1$; $Pr = 1$; $M = 1$; $Re = 2$, $\phi_1 = 1$; $\phi_2 = 1$; Z = 1.

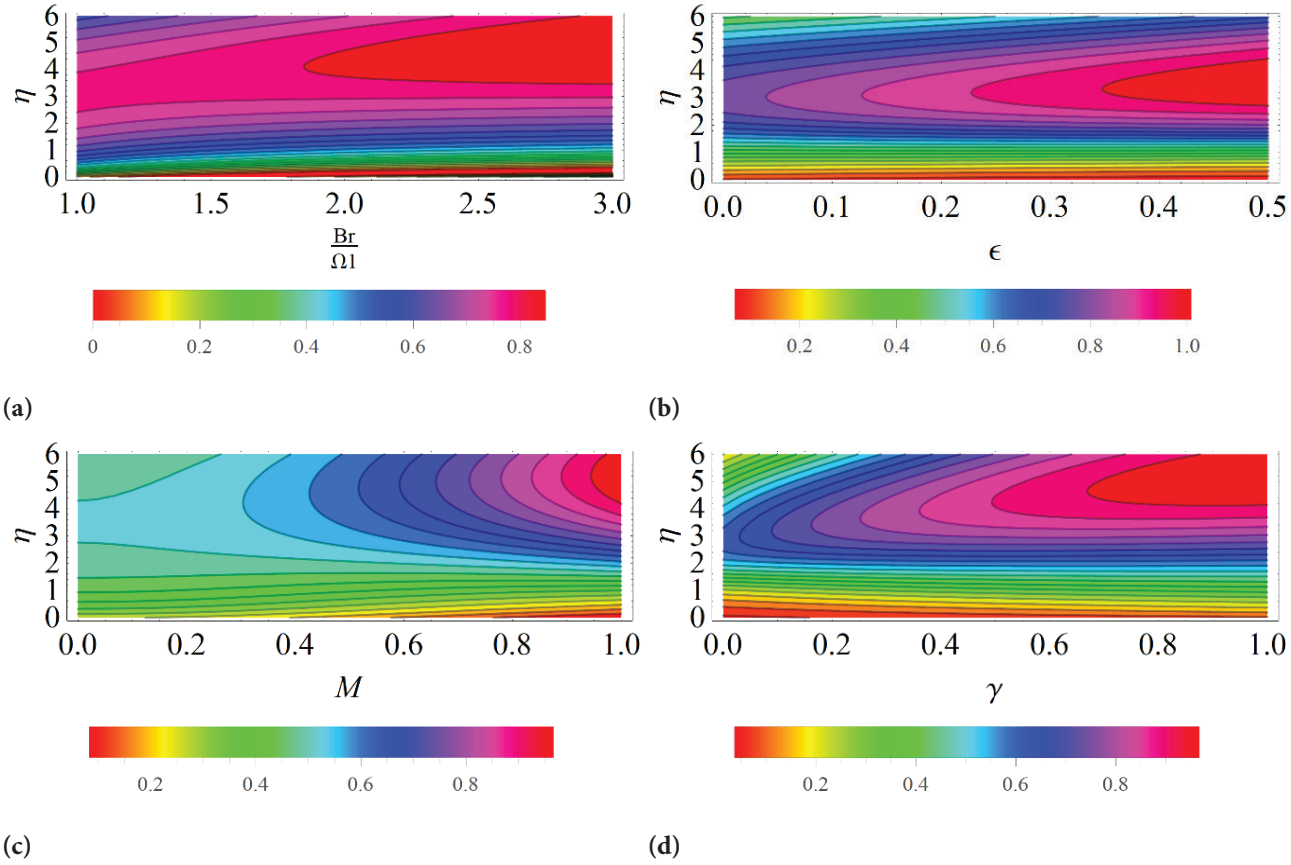

Figure 8. Contour plot for Bejan with (a) distinct modified Brinkman number (b) distinct ε (c) distinct M (d) distinct γ, when $Gr_t = 0.3$; $Gr_c = 0.3$; $\alpha = \pi/4$; $Q = 0.3$; $\varepsilon = 0.1$; $Nb = 0.1$; $Nt = 0.1$; $Br = 0.35$; $Df = 0.5$; $Sc = 0.5$; $Sr = 0.5$; $C_r = 0.3$; $\gamma = 1$; $Pr = 1$; $M = 1$; $Re = 2$, $\phi_1 = 1$; $\phi_2 = 1$; Z = 1.

Table 1. Comparison of the numerical solution with Bvph 2.0 when $\gamma = 0.1$; $Pr = 0.7$; $M = 1$; $Gr_t = 0.7$; $Gr_c = 0.2$; $\alpha = \pi/4$; $Q = 0.1$; $\epsilon = 0.1$; $Nb = 0.1$; $Nt = 0.1$; $Br = 0.35$; $Df = 0.5$; $Sc = 0.5$; $Sr = 0.5$; $C_r = 0.3$

η	f' (η)			θ(η)			ϕ(η)		
	Numerical (NDSolve)	HAM Bvph 2.0	ERROR	Numerical (NDSolve)	HAM Bvph 2.0	ERROR	Numerical (NDSolve)	HAM Bvph 2.0	ERROR
0	1	1	0.00000	1	1	0.00000	-0.338485	-0.297767	0.040718
1	0.340713	0.350775	0.010062	0.476101	0.493397	0.017296	0.0889137	0.121118	0.032204
2	0.148851	0.167530	0.018679	0.243882	0.278084	0.034202	0.156769	0.187434	0.030665
3	0.0739229	0.099781	0.025858	0.131425	0.1795028	0.048078	0.126402	0.160192	0.03379
4	0.0361215	0.067316	0.031195	0.0673214	0.125667	0.058346	0.0810324	0.123622	0.04259
5	0.0138076	0.048495	0.034687	0.0267878	0.091770	0.064982	0.0383084	0.0936327	0.055324
6	0	0.036261	0.036261	0	0.068445	0.068445	0	0.0708699	0.07087

the stretching pipe is dominated by viscosity and magnetic irreversibility.

Table 1 shows that both the techniques, numerical solution by shooting technique with Gill's fourth order method, and Bvph2.0 suits each other. From Table 2, we observed that the drag force at the walls/ surfaces, heat transfer rate increases, and mass transfer rate decreases for increasing values of γ, Pr, Nt, Df. For increasing values of α, the skin friction, Sherwood number increases and Nusselt number decreases. The drag force at the walls/ surfaces, Sherwood number decreases, and heat transfer rate increases for increasing values of ε, Nb, Sr.

Table 2. Numerical values of $-f''(0)$, $-\theta'(0)$, $-\phi'(0)$ at $M = 1$; $Gr_t = 0.7$; $Gr_c = 0.2$; $Q = 0.1$; $C_r = 0.3$; $Sc = 0.5$

γ	α	*Nb*	*Nt*	*Sr*	*Df*	*Pr*	ε	$-f''(0)$	$-\theta'(0)$	$-\phi'(0)$
0.1				0.5	0.5		0.1	1.2242	0.7241	-0.7241
0.3	π/4	0.1	0.1	0.5	0.5	0.7	0.1	1.3186	0.7916	-0.7916
0.5								1.4084	0.8548	-0.8548
	π/6							1.1752	0.7508	-0.7508
0.1	π/4	0.1	0.1	0.5	0.5	0.7	0.1	1.2242	0.7241	-0.7241
	π/3							1.2897	0.6858	-0.6858
						0.7		1.2242	0.7241	-0.7241
0.1	π/4	0.1	0.1	0.5	0.5	1.3	0.1	1.2461	0.9676	-0.9676
						1.6		1.2637	1.2756	-1.2756
		0.1						1.2242	0.7241	-0.7241
0.1	π/4	0.3	0.1	0.5	0.5	0.7	0.1	1.2023	0.6070	0.2023
		0.5						1.1981	0.5883	0.1177
			0.1					1.1962	0.5804	-0.0829
0.1	π/4	0.7	0.3	0.5	0.5	0.7	0.1	1.2035	0.6102	-0.2615
			0.5					1.2110	0.6455	-0.4611
				0.5				1.2242	0.7241	-0.7241
0.1	π/4	0.1	0.1	1	0.5	0.7	0.1	1.2139	0.7404	-0.7404
				1.5				1.2028	0.7576	-0.7576
					0.5			1.2242	0.7241	-0.7241
0.1	π/4	0.1	0.1	0.5	0.8	0.7	0.1	1.2369	0.9025	-0.9025
					1			1.2462	1.1098	-1.1098
							0.1	1.2242	0.7241	-0.7241
0.1	π/4	0.1	0.1	0.5	0.5	0.7	0.3	1.2165	0.6217	-0.6217
							0.5	1.2095	0.5518	-0.5518

CONCLUSION

The impacts of variable thermal conductivity, entropy generation rate, heat transfer rate, Soret and Dufour parameters in nanofluid flow over inclined stretching cylinder are studied under the influence of viscous dissipation and internal heat source using Buongiorno model. The major findings are concluded as;

(i) The higher intensity of the magnetic field (M = 0, 1, 2) decreases axial velocity and concentration, but a reverse trend appears for the temperature field. This is happening due to the force generated in the opposite direction to the flow.

(ii) The temperature profile rises with increasing values of ϵ, γ ($0 \le \gamma \le 1$) and decelerates with α, *Sr,* and *Df*. Rise of temperature produces more mass transfer that disturbs the energy of the system. This effect needs to administer the entropy.

(iii) The axial velocity decelerates with inclination angle ($\pi/6 \le \alpha \le \pi/3$) increases. The inclination angle is affecting the flow transport rate that will create the major change in the energy of the system that will be leading cause of administering the entropy of the system.

(iv) The concentration distribution increases for a given increase in *Sr,* and decrease in M, γ.

(v) Entropy increases with magnetic parameter, curvature parameter, group parameter, and variable thermal conductivity.

(vi) Bejan number increases with increase of γ, ϵ, and M and decreases with group parameter.

It is observed that some parameters like magnetic field, curvature, group, and variable thermal conductivity increase entropy that will increase the energy of the system. Higher energy in the system will create the disorder. This disorder causes more turbulence in physical systems, especially in biological processes. From the administrative/clinical point of view entropy must be optimized that will be good for the industrial, medical, and clinical applications.

Future Scope

The mathematical techniques employed to solve the current physical model exhibit great agreement with the past research that are now available, which supports the veracity of the current physical findings. Engineers can benefit from this paper's extension to hybrid nanofluid or two-phase fluids based on these findings. Engineers have

good options for comparing the amount of heat released by the system due to nanoparticle movements in thermal processes experimentally and theoretically.

NOMENCLATURE

Be	Bejan number
Br	Brinkman number
B_o	constant magnetic field
C	fluid concentration (kg/m^3)
C_∞	ambient nanoparticle concentration
C_p	specific heat (J/kg-K)
C_p^*	specific heat of nanofluid
C_s	concentration susceptibility
C_r	Chemical reaction parameter
C_w	Concentration at the surface
D	molecular diffusivity (m^2 /s)
D_B	Brownian diffusion coefficient (m^2 /s)
D_T	thermophoresis diffusion coefficient (m^2 /s)
Df	Dufour number
Ec	Eckert number
g	gravitational acceleration (m/s^2)
Gr_c	Local concentration Grashof number
Gr_t	Local temperature Grashof number
k	thermal conductivity (Wb/m^2)
k_1	Rate of reaction
k_T	Thermal diffusion ratio
l	the characteristic length(m)
M	Magnetic field number(W/mK)
Nb	Brownian motion parameter
Nt	Thermophoretic parameter
Pr	Prandtl number
Ns	Non dimensional Entropy generation number
Q	heat source/sink parameter
Q_o	heat coefficient
Re	Reynolds number
Re_z	local Reynolds number
Sc	Schmidt number
S_G	Entropy generation
T	fluid temperature(K)
T_m	Mean temperature(K)
T_0	reference temperature(K)
T_w	Temperature at the surface(K)
T_∞	ambient temperature(K)
(r, z)	Radial and axial coordinates in cylindrical system
U_0	reference velocity
(u, w)	velocity components in the (r, z) direction(m/s)

Greek Symbols

α	Angle of inclination
β_T	the thermal expansion coefficient
β_C	concentration expansion coefficient
ϵ	Thermal conductivity parameter
μ	dynamic viscosity of fluid(Pa.s)
ρ	density of fluid(Kg/m^3)
ρ*	density of nanofluid
η	Similarity variable
σ*	Stefan–Boltzmann constant
γ	cylinder curvature parameter
ν	kinematic viscosity
σ	electrical conductivity (or specific conductance) (S/m)
θ	dimensionless temperature
ϕ	dimensionless concentration
Ω_1, Ω_2	Temperature and concentration difference coefficient
ϕ_1, ϕ_2	irreversibility distribution ratios

ACKNOWLEDGEMENT

The conduct of this research study is not currently supported by any funding source.

AUTHORSHIP CONTRIBUTIONS

Authors equally contributed to this work.

DATA AVAILABILITY STATEMENT

The authors confirm that the data that supports the findings of this study are available within the article. Raw data that support the finding of this study are available from the corresponding author, upon reasonable request.

CONFLICT OF INTEREST

The author declared no potential conflicts of interest with respect to the research, authorship, and/or publication of this article.

ETHICS

There are no ethical issues with the publication of this manuscript.

REFERENCES

[1] Choi US. Enhancing thermal conductivity of fluids with nanoparticles, developments and applications of non-Newtonian flows. ASME J Heat Transf 1995;231:99-105.

[2] Buongiorno J. Convective transport in nanofluids. J Heat Transf 2006;128:240-250. [CrossRef]

[3] Nield DA, Kuznetsov AV. The Cheng-Minkowycz problem for natural convective boundary-layer flow in a porous medium saturated by a nanofluid. Int J Heat Mass Transf 2009;52:5792-5795. [CrossRef]

[4] Mansur S, Ishak A. The flow and heat transfer of a nanofluid past a stretching/shrinking sheet with a convective boundary condition. Abstr Appl Anal 2013;2013:350647. [CrossRef]

[5] Kuznetsov AV, Nield DA. Natural convective boundary-layer flow of a nanofluid past a vertical plate. Int J Therm Sci 2010;49:243-247. [CrossRef]

[6] Rana GC, Thakur RC. The onset of double-diffusive convection in a layer of nanofluid under rotation. Rev Eng Térmica 2016;15:88. [CrossRef]
[7] Narla VK, Tripathi D, Bég OA. Analysis of entropy generation in biomimetic electroosmotic nanofluid pumping through a curved channel with joule dissipation. Therm Sci Engineer Prog 2020;15:100424. [CrossRef]
[8] Mahatha BK, Nandkeolyar R, Nagaraju G, Das M. MHD stagnation point flow of a nanofluid with velocity slip, non-linear radiation and Newtonian heating. Procedia Engineer 2015;127:1010-1017. [CrossRef]
[9] Nagaraju G, Jangili S, Ramana Murthy JV, Bég OA, Kadir A. Second law analysis of flow in a circular pipe with uniform suction and magnetic field effects. J Heat Transf 2019;141:012004. [CrossRef]
[10] Mondal H, Das S, Kundu PK. Influence of an inclined stretching cylinder over MHD mixed convective nanofluid flow due to chemical reaction and viscous dissipation. Heat Transf 2020;49:2183-2193. [CrossRef]
[11] Kandwal S, Mishra A, Kumar M. Numerical investigation of nanofluid heat transfer in an inclined stretching cylinder under the influence of suction/injection and viscous dissipation. Nanosci Technol An Int J 2019;10:29-49. [CrossRef]
[12] Elbashbeshy EMA, Emam TG, Abdel-wahed MS. Effect of heat treatment process with a new cooling medium (nanofluid) on the mechanical properties of an unsteady continuous moving cylinder. J Mech Sci Technol 2013;27:3843-3850. [CrossRef]
[13] Bisht V, Kumar M, ZU. Effects of variable thermal conductivity and chemical reaction on steady mixed convection boundary layer flow with heat and mass transfer inside a cone due to a point sink. J Appl Fluid Mech 2011;4:59-63. [CrossRef]
[14] Ravi Kanth ASV, Kumar NU. A haar wavelet study on convective-radiative fin under continuous motion with temperature-dependent thermal conductivity. Walailak J Sci Technol 2014;11:211-224.
[15] Salahuddin T, Malik MY, Hussain A, Bilal S, Awais M. Combined effects of variable thermal conductivity and MHD flow on pseudoplastic fluid over a stretching cylinder by using Keller Box method. Inf Sci Lett 2016;5:11-19. [CrossRef]
[16] Ramzan M, Bilal M, Kanwal S, Dong CJ. Effects of variable thermal conductivity and non-linear thermal radiation past an Eyring Powell nanofluid flow with chemical reaction. Comm Theor Phys 2017;67:723. [CrossRef]
[17] Gajjela N, Garvandha M. Impacts of variable thermal conductivity and mixed convective stagnation-point flow in a couple stress nanofluid with viscous heating and heat source. Heat Transf 2020;49:3630-650. [CrossRef]
[18] Sakiadis BC. Boundary-layer behavior on continuous solid surfaces: I. Boundary-layer equations for two-dimensional and axisymmetric flow. AIChE J 1961;7:26-28. [CrossRef]
[19] Crane LJ. Boundary layer flow due to a stretching cylinder. ZAMP Zeitschrift Für Angew Math Und Phys 1975;26:619-622. [CrossRef]
[20] Wang CY. Fluid flow due to a stretching cylinder. Phys Fluids 1988;31:466-468. [CrossRef]
[21] Gorla RSR, Chamkha AJ, Al-Meshaiei E. Melting heat transfer in a nanofluid boundary layer on a stretching circular cylinder. J Nav Archit Mar Engineer 2012;9:1-10. [CrossRef]
[22] Dhanai R, Rana P, Kumar L. MHD mixed convection nanofluid flow and heat transfer over an inclined cylinder due to velocity and thermal slip effects: Buongiorno's model. Powder Technol 2016;288:140-150. [CrossRef]
[23] El-Kabeir SMM. Soret and Dufour effects on heat and mass transfer by mixed convection over a vertical surface saturated porous medium with temperature dependent viscosity. Int J Numer Methods Fluids 2012;69:1633-1645. [CrossRef]
[24] Dzulkifli NF, Bachok N, Pop I, Yacob NA, Md Arifin N, Rosali H. Soret and Dufour effects on unsteady boundary layer flow and heat transfer of nanofluid over a stretching/shrinking sheet: A stability analysis. J Chem Engineer Process Technol 2017;08:1000336. [CrossRef]
[25] Gajjela N, Matta A, Kaladhar K. The effects of Soret and Dufour, chemical reaction, Hall and ion currents on magnetized micropolar flow through co-rotating cylinders. AIP Adv 2017;7:115201. [CrossRef]
[26] Jain S, Bohra S. Soret/Dufour effects on radiative free convection flow and mass transfer over a sphere with velocity slip and thermal jump. Walailak J Sci Technol 2018;16:701-721. [CrossRef]
[27] Gajjela N, Garvandha M. The influence of magnetized couple stress heat, and mass transfer flow in a stretching cylinder with convective boundary condition, cross-diffusion, and chemical reaction. Therm Sci Engineer Prog 2020;18:100517. [CrossRef]
[28] Idowu AS, Falodun BO. Effects of thermophoresis, Soret-Dufour on heat and mass transfer flow of magnetohydrodynamics non-Newtonian nanofluid over an inclined plate. Arab J Basic Appl Sci 2020;27:149-165. [CrossRef]
[29] Bejan A, Kestin J. Entropy generation through heat and fluid flow. J Appl Mech 1983;50:475. [CrossRef]
[30] Butt AS, Ali A, Mehmood A. Numerical investigation of magnetic field effects on entropy generation in viscous flow over a stretching cylinder embedded in a porous medium. Energy 2016;99:237-249. [CrossRef]
[31] Srinivasacharya D, Shafeeurrahman M. Joule heating effect on entropy generation in MHD mixed convection flow of chemically reacting nanofluid

between two concentric cylinders. Int J Heat Technol 2017;35:487-497. [CrossRef]

[32] Taghizadeh S, Asaditaheri A. Heat transfer and entropy generation of laminar mixed convection in an inclined lid driven enclosure with a circular porous cylinder. Int J Therm Sci 2018;134:242-257. [CrossRef]

[33] Tufail MN, Butt AS, Dar A, Ali A. Theoretical investigation of entropy generation effects in nanofluid flow over an inclined stretching cylinder. Int J Exergy 2019;28:126. [CrossRef]

[34] Zheng Y, Yaghoubi S, Dezfulizadeh A, Aghakhani S, Karimipour A, Tlili I. Free convection/radiation and entropy generation analyses for nanofluid of inclined square enclosure with uniform magnetic field. J Therm Anal Calorim 2020;141:635-648. [CrossRef]

[35] Jha BK, Yusuf TS. Entropy generation in an inclined porous channel with suction/injection. Nonlinear Eng 2019;9:94-104. [CrossRef]

[36] Sahoo A, Nandkeolyar R. Entropy generation and dissipative heat transfer analysis of mixed convective hydromagnetic flow of a Casson nanofluid with thermal radiation and Hall current. Sci Rep 2021;11:3926. [CrossRef]

[37] Zahor FA, Jain R, Ali AO, Masanja VG. Modeling entropy generation of magnetohydrodynamics flow of nanofluid in a porous medium: a review. Int J Numer Methods Heat Fluid Flow 2023;33:751-771. [CrossRef]

[38] Raje A, Bhise AA, Kulkarni A. Entropy analysis of the MHD Jeffrey fluid flow in an inclined porous pipe with convective boundaries. Int J Thermofluids 2023;17:100275. [CrossRef]

[39] Teh YY, Ashgar A. Three dimensional MHD hybrid nanofluid flow with rotating stretching/shrinking sheet and joule heating. CFD Lett 2021;13:1-19. [CrossRef]

[40] Ferroudj N, Köten H. Numerical simulation of prandtl number effect on entropy generation in a square cavity. J Therm Engineer 2021;7:1016-1029. [CrossRef]

[41] Sharma BK, Sharma P, Mishra NK, Noeiaghdam S, Fernandez-Gamiz U. Bayesian regularization networks for micropolar ternary hybrid nanofluid flow of blood with homogeneous and heterogeneous reactions: entropy generation optimization. Alex Engineer J 2023;77:127-148. [CrossRef]

[42] Mishra NK, Sharma M, Sharma BK, Khanduri U. Soret and Dufour effects on MHD nanofluid flow of blood through a stenosed artery with variable viscosity. Int J Mod Phys B 2023;37:2350266. [CrossRef]

[43] Paul A, Nath JM, Das TK. An investigation of the MHD Cu-Al2O3/H2O hybrid-nanofluid in a porous medium across a vertically stretching cylinder incorporating thermal stratification impact. J Therm Engineer 2023:799-810. [CrossRef]

[44] Zhao Y, Liao S. Chapter 9: HAM-based Mathematica package BVPh 2.0 for nonlinear boundary value problems. Adv Homotopy Anal Method, World Scientific 2014:361-417. [CrossRef]